Engineering Notes

ENGINEERING NOTES are short manuscripts describing new developments or important results of a preliminary nature. These Notes cannot exceed 6 manuscript pages and 3 figures; a page of text may be substituted for a figure and vice versa. After informal review by the editors, they may be published within a few months of the date of receipt. Style requirements are the same as for regular contributions (see inside back cover).

Body of Revolution Comparisons for Axial- and Surface-Singularity Distributions

Joseph M. D'Sa* and Charles Dalton†
University of Houston, Houston, Texas

Introduction

A GIVEN axisymmetric body immersed in an incompressible uniform flow can be represented by two different types of singularity methods. The simpler type is the method of axial singularities. This representation is by a distribution of line sources and sinks aligned with the uniform flow to form the closed body shape. The surface of the body is represented by a constant value of stream function, typically taken to be zero. The more complex, but far more versatile, technique is the method of surface-distributed singularities which are typically ring sources and sinks, but can also be ring doublets or vortices. The surface-distribution method is more complex because the method of describing the body involves control points which are also singular.

In the following discussion, a comparison of the surface velocities generated by the two different methods will be made. It will be shown that the simplicity of the axial-singularity method is actually its major problem in representing axisymmetric body shapes. It will also be evident that the complexity of the surface-singularity method is its strength in representing axisymmetric body shapes.

Analysis

Axial Singularities

In one of its earliest applications, Rankine[1] used the axial-singularity method to represent the calculation of streamlines on axisymmetric bodies. von Kármán[2] used the axial-singularity method to represent the flowfield about airship hulls. Recently, there have been numerous studies utilizing axial singularities to represent axisymmetric bodies. These studies typically have addressed singularity distributions using a constant strength over the element length. One of the more relevant studies was presented by Oberkampf and Watson.[3] They recognized that the axial-singularity method produced a generally ill-conditioned coefficient matrix. Oberkampf and Watson showed that the performance of the axial-singularity method is sensitive to both the number of elements and the body geometry. Zedan and Dalton[4] showed that the constant-strength method of Ref. 3 fails for nonsymmetrical bodies about the midsection plane. The use of a linearly varying singularity distribution allowed Zedan and Dalton to remove the symmetry restriction and improve the accuracy of the method in general with the same memory requirement and a negligible increase in computing time. The accuracy of the method using linearly varying strength elements was still questionable near the tail for bodies with an inflection point in the meridional curve.

To resolve the problems encountered by Zedan and Dalton,[4] they developed a continuously varying strength distribution description of the axial singularities.[5] In Ref. 5, it was found that a combination of 11 elements with linear intensity variation and 5 elements with a parabolic strength variation provided an accuracy that compared favorably to the surface-singularity method with 47 elements.

The stream function for a continuously varying distribution of source/sink strength is given by

$$\psi(\xi,\zeta)=\frac{-1}{4\pi}\int_0^{\ell}\frac{(\xi-\zeta)\sigma_\zeta \mathrm{d}\zeta}{[(\xi-\zeta)^2+\eta^2]^{1/2}}+U_\infty\frac{r^2}{2} \tag{1}$$

and the velocity components are

$$u(\xi,\zeta)=\frac{1}{4\pi}\int_0^{\ell}\frac{(\xi-\zeta)\sigma_\zeta \mathrm{d}\zeta}{[(\xi-\zeta)^2+\eta^2]^{3/2}}+U_\infty \tag{2}$$

and

$$v(\xi,\eta)=\frac{\eta}{4\pi}\int_0^{\ell}\frac{\sigma_\zeta \mathrm{d}\zeta}{[(\xi-\zeta)^2+\eta^2]^{3/2}} \tag{3}$$

The notation and geometry used here are the same as in Ref. 5. Equations (1-3) can be restated in terms of a one-dimensional array of unknown strength distributions C_j,

$$\psi_i=\frac{1}{4\pi}\sum_{j=1}^{M}\Psi_{ij}C_j+\frac{U_\infty r_i^2}{2} \tag{4}$$

$$u_i=\frac{1}{4\pi}\sum_{j=1}^{M}U_{ij}C_j+U_\infty \tag{5}$$

and

$$v_i=\frac{n_i}{4\pi}\sum_{j=1}^{M}V_{ij}C_j \tag{6}$$

The array C_j represents the source/sink values to be determined and the quantities Ψ_{ij}, U_{ij}, and V_{ij} are geometry-dependent. The σ_ζ variation in Eqs. (1-3) has been replaced by the nth-degree polynomial

$$\sigma_\zeta=\sum_{k=1}^{m+1}a_k\zeta^{k-1} \tag{7}$$

which represents the source/sink intensity over each element. Further details of the description may be found in Ref. 5.

Surface Singularities

Kellogg[6] presented the basis for the surface-singularity method. The velocity potential ϕ at a point P due to a body

Received Oct. 29, 1985; revision received March 31, 1986.

*Graduate Assistant, Department of Mechanical Engineering.
†Professor of Mechanical Engineering and Associate Dean of Engineering.

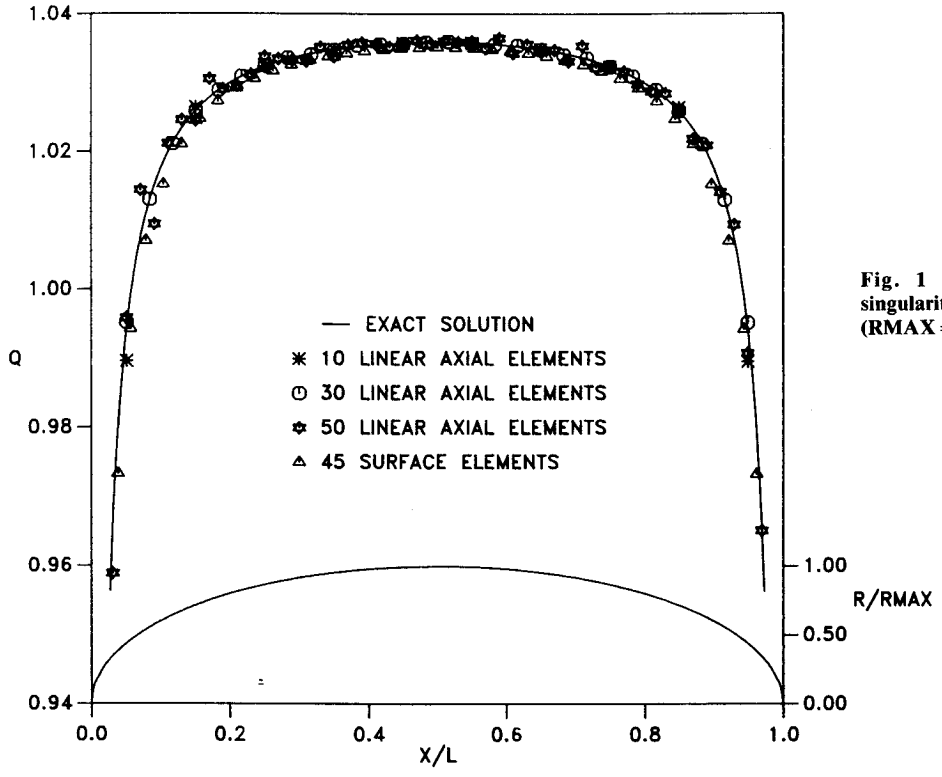

Fig. 1 Comparison between exact, surface-singularity, and linear axial-singularity solutions (RMAX = maximum radius).

shell S is given by

$$\phi(P) = \int_S \frac{1}{r}\sigma(q)\mathrm{d}S \tag{8}$$

where $\sigma(q)$ is the singularity distribution (source or sink), q a point on the body surface, and r the distance between P and q. Use of this potential leads to the Neumann problem where the body surface is described by the no-penetration boundary condition. Smith and Pierce[7] have treated this problem for a ring source of radius a and singularity distribution σ. If the ring source is located at $x=b$ with its center at $(b,0,0)$, then the velocities are given by

$$\left(\frac{\partial\phi}{\partial x}\right)_P = \int_0^S \frac{-4a(x-b)\sigma E(k)\mathrm{d}s}{[(y-a)^2+(x-b)^2][(y+a)^2+(x-b)^2]^{1/2}} \tag{9}$$

and

$$\left(\frac{\partial\phi}{\partial y}\right)_P = \int_0^S \left[K(k) + \frac{(y^2-a^2)-(x-b)^2}{(y-a)^2+(x-b)^2}E(k)\right] \times \frac{(-2\alpha\sigma)\mathrm{d}s}{y[(y+a)^2+(x-b)^2]^{1/2}} \tag{10}$$

where $\mathrm{d}s$ is a differential element of length along the surface, S is the total meridional length, $k^2 = 4ay/[(x-b)^2 + (y+a)^2]$, and $E(k)$ and $K(k)$ are complete elliptic integrals of the first and second kind, respectively.

Smith and Pierce present a detailed analysis of the surface-singularity method for flow about plane and axisymmetric bodies. Their analysis determines the derivatives of the source/sink potential for an external flow at a point exterior to the body. The velocity components are given by

$$\frac{\partial\phi}{\partial x_+} = 2\pi\sigma_+\sin\alpha + \frac{\partial\phi}{\partial x} \tag{11}$$

and

$$\frac{\partial\phi}{\partial y_+} = -2\pi\sigma_+\cos\alpha + \frac{\partial\phi}{\partial y} \tag{12}$$

where the quantities $\partial\phi/\partial x$ and $\partial\phi/\partial y$ represent the contributions from the entire surface except for the singular points, and σ_+ represents the external local surface value of the singularity distribution. The derivatives $\partial\phi/\partial x$ and $\partial\phi/\partial y$ are determined solely from the body geometry and the value of the source/sink ring singularities at each body increment. The surface-singularity geometry consists of a series of frustums with flat lateral surfaces and a constant-singularity distribution over each frustum surface.

These velocities in Eqs. (11) and (12) are next put into normal and tangential components. The values of the source/sink singularity distributions are determined from the zero normal-velocity component. The tangential-velocity distribution is then obtained from these source/sink singularity distributions. Further details are found in Ref. 7.

Results

The axial- and surface-singularity methods were compared by performing calculations of an ellipsoid of revolution fineness ratio (FR) of 7 and the David Taylor Naval Ship Research and Development Center (DTNSRDC) afterbody.[8] The reason for selecting the ellipsoid of revolution was the simplicity of its meridional profile and the availability of the exact solution. On the other hand, the body of Ref. 8 shows a variety of aspects in its meridional profile, i.e., a rounded nose, a flat midsection, an inflection between the midsection and the tail, and a rounded tail.

For the ellipsoid of revolution ($FR=7$), results using the axial-singularity method show the following: As few as 10 (linearly or parabolically varying) elements satisfactorily represent the body and predict the tangential velocity on the body. For more than 35 linearly varying or parabolically varying elements, the method shows deviations in the tangential velocity on the body. Results for the surface-singularity method as applied to the ellipsoid of revolution of $FR=7$

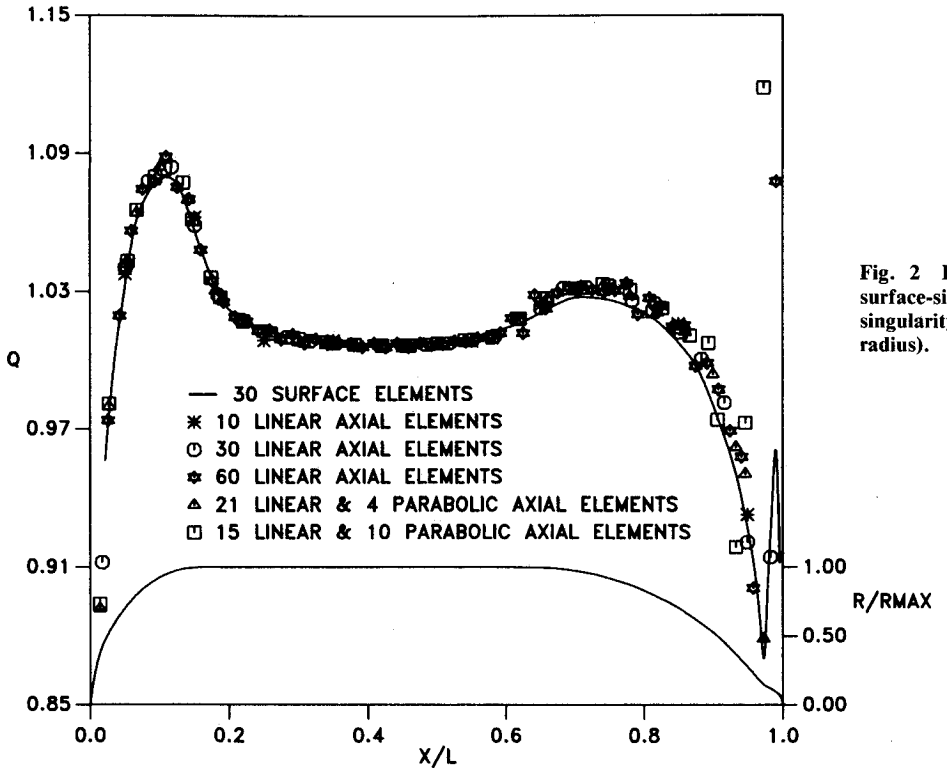

Fig. 2 DTNSRDC afterbody 1 results showing surface-singularity and linear and parabolic axial-singularity element solutions (RMAX = maximum radius).

show that it takes a minimum of 45 elements to obtain a good representation of the body and satisfactorily predict the tangential velocity on the body. Increasing the number of surface elements to 70 only goes to improve the representation of the body and the prediction of the tangential velocity. See Fig. 1.

Next, the body of Ref. 8 serves as an example to compare the axial- and surface-singularity methods. Since the surface-singularity method proved to be the better of the two methods for the ellipsoid of revolution, it represents the standard to which the axial-singularity results will be compared. The surface-singularity method produced a smooth velocity profile when 30 constant-strength surface-source elements were used. When 25 panels were used, the results showed a deviation from the velocity distribution obtained for 30 or more elements. Increasing the number of elements to as many as 70 produced no change in the velocity distribution. The result for the 30-panel case is shown in Fig. 2.

The axial-singularity representation of the body in Ref. 8 produces the comparison case. There are several comparisons to be made for this situation. For a low number of linearly varying elements (10 or less), the method does not work well because the trailing edge is not adequately represented. When the number of linearly varying elements is high (more than 30), the method shows an instability in the solution for the rear half of the body with the instability moving toward the front as the number of elements increases. Also, for the greater number of elements, the method is able to detect the inflection point in the body shape, but the rear stagnation point is not represented satisfactorily. The best distribution of the body was given by the 20-element solution. No axial-singularity solution was found to describe the body adequately at the rear stagnation point. All of the solutions attempted produced a velocity distribution which diverged at the trailing edge of the body. These comparisons are shown in Fig. 2.

The next comparison involves the axial singularities for parabolically varying strengths. Ten elements gave a fair representation of the body shape except near the rear. The parabolic representation develops an instability as the number of elements increases past 20. These comparisons are not shown.

A combination of linearly and parabolically varying strengths was conjectured to give a more accurate solution to the representation of the body of Ref. 8. With 5 parabolic elements at each end and 15 intermediate linear elements, the solution was found to be extremely unstable at the rear of the body. Reducing the number of parabolic elements to two on each end, but keeping the total number of elements the same caused the perturbations to be damped but the deviation at the rear stagnation point remained large. These results are also shown in Fig. 2.

In order to take the slope of the body profile into consideration, the problem was solved using the no-penetration boundary condition instead of the constant stream function boundary condition. For the linearly varying axial singularities, the method is unable to represent the body for the 10-element distribution due to the extensive perturbations in the solution for the tangential velocity along the entire body. Increasing the number of elements decreases the perturbations along most of the body but increases the perturbations at the rear end. The parabolically varying elements were unable to represent the body due to perturbations in the solution even when the number of elements was low. These results are also not shown graphically.

Conclusions

In conclusion, it is noted that, of all of the axial-singularity representations of the two bodies, the linearly varying axial-singularity method was the best. Although the parabolically varying axial-singularity method worked satisfactorily for the simpler body, it was unable to do so for the complex body, showing an inconsistency in its application. Even for the linearly varying axial-singularity method, selection of the number of elements becomes critical as the geometry of the body becomes complex. For instance, the range of the number of elements for satisfactory application of the method was from 10 to 35 for the ellipsoid of revolution and from 20 to 30 for the body of Ref. 8. The surface-singularity method, on the other hand, requires a relatively

larger number of points to represent adequately the geometry of a body. This and other reasons—such as the numerical integration over each element of the body surface—increase the computing time for this method. However, its ability to represent even complex body shapes makes it the superior method.

References

[1]Rankine, W. J. M., "On the Mathematical Theory of Stream Lines, Especially Those with Four Foci and Upwards," *Philosophical Transactions of the Royal Society of London,* Vol. 161, Pt. II, 1871, pp. 267-306.

[2]von Kármán, T., "Calculation of Pressure Distribution on Airship Hulls," NACA TM 574, 1930.

[3]Oberkampf, W. L. and Watson, L. E., "Incompressible Potential Flow Solutions for Arbitrary Bodies of Revolution," *AIAA Journal*, Vol. 12, March 1974, pp. 409-411.

[4]Zedan, M. F. and Dalton, C., "Potential Flow Around Axisymmetric Bodies: Direct and Inverse Problems," *AIAA Journal,* Vol. 16, March 1978, pp. 242-250.

[5]Zedan, M. F., and Dalton, C., "Higher Order Axial Singularity Distributions for Potential Flow About Bodies of Revolution," *Computer Methods in Applied Mechanics and Engineering,* Vol. 21, March 1980, pp. 295-314.

[6]Kellogg, O. D., *Foundation of Potential Theory,* Dover Publishers, NY, 1953 (original edition, 1929).

[7]Smith, A. M. O. and Pierce, J., "Exact Solution of the Neumann Problem. Calculation of Non-Circulatory Plane and Axially Symmetric Flows About or Within Arbitrary Boundaries," Douglas Aircraft Co., Long Beach, CA, Rept. ES 26988, 1958.

[8]Huang, T. T., Santelli, N., and Belt, G., "Stern Boundary-Layer Flow on Axisymmetric Bodies," *Proceedings of the 12th Symposium on Naval Hydrodynamics,* Office of Naval Research, Washington, DC, June 1978, pp. 127-157.